Neutron emission in the fissioning ^{158}Er composite system

A. Gavron, A. Gayer, J. Boissevain, and H. C. Britt
Los Alamos National Laboratory, Los Alamos, New Mexico 87545

T. C. Awes, J. R. Beene, B. Cheynis, D. Drain, R. L. Ferguson, F. E. Obenshain, F. Plasil, and G. R. Young
Oak Ridge National Laboratory, Oak Ridge, Tennessee 37831

G. A. Petitt and C. Butler
Georgia State University, Atlanta, Georgia 30303
(Received 9 October 1986)

We have measured the spectra and angular distribution of neutrons emitted in coincidence with fission fragments in the following reactions: $^{16}O+^{142}Nd$ ($E_{beam}=207$ MeV), $^{24}Mg+^{134}Ba$ (180 MeV), $^{32}S+^{126}Te$ (180 MeV), and $^{50}Ti+^{108}Pd$ (216 MeV). We decompose neutron emission into components resulting from nonequilibrium emission, emission from the compound system, and emission from the fission fragments. We find that statistical model calculations tend to underestimate the number of neutrons evaporated prior to fission. Incorporating the effects of (1) the finite time until equilibrium fission probability is attained at the saddle point, (2) correction to the Bohr-Wheeler formalism due to nuclear viscosity, and (3) neutron emission during the descent from saddle to scission, improves the agreement with the experimental data. The value of the reduced nuclear dissipation coefficient β that is consistent with our data is approximately 6×10^{21} s^{-1}, within the framework of the model we have used.

I. INTRODUCTION

During the past few years, several groups have invested an extensive effort in measurements of particle emission associated with heavy-ion fission reactions.[1-11] Various problems have been addressed by these studies, such as limits to the statistical model at high temperature and angular momentum, the time scale of fusion and fission, and the existence of "quasi-fission."[12-15]

Details of studies of charged particle emission are presented in Refs. 9—11 and the references therein. Various sources of particles have been inferred; the dominant ones are evaporation from the composite system prior to fission and evaporation from the fully accelerated fission fragments. Evaporation from the composite system is significant even in the $^{40}Ar+^{238}U$ reaction at 334 MeV, where the fission barrier is essentially zero, even though no such emission would be expected on the basis of statistical model calculations. These results present evidence for fission times that are long compared to particle evaporation times at high excitation energies. Additional sources for particle emission which have been inferred are "neck" emission[9,11] (similar to long range alpha particles in low energy fission) and nonequilibrium emission.[10,11] Attempts have been made to use charged particle emission to determine the lifetime of the composite system: Schad *et al.*[11] observe nuclear shadowing for sequential emission from the fragments and estimate a composite system lifetime of $(1-3)\times10^{-20}$ s for 218 MeV excited ^{143}Gd. Duek *et al.*[9] detect enhanced alpha particle emission from mass-symmetric fission and find it compatible with the possibility that mass asymmetric fission is a faster process.

Extensive studies of neutron emission of heavy-ion fission reactions are reported in Refs. 1—8. The dominant feature of these results is that neutrons, like charged particles,[9] seem to be evaporated prior to fission with multiplicities significantly exceeding statistical model estimates. For the heavier systems, Hinde *et al.*[7] interpret these neutrons as resulting from emission by the fragments during the initial stages of their acceleration. However, this interpretation is not adequate for lighter systems;[2,5,8] Hinde *et al.*[8] consider several composite systems with Z between 70 and 99. They use statistical model calculations in which they include effects of a delayed onset of fission and a slow saddle-to-scission transition time. During these times neutrons are emitted without fission competition and are detected as prefission neutrons in the experimental apparatus. The delay times they use are consistent with results obtained using one body dissipation.[16] Zank *et al.*[5] attribute the entire excess neutron emission to the long transition time between the saddle and the scission point. The nuclear dissipation coefficient necessary to reproduce such a long time is an order of magnitude larger than the value obtained by Davies *et al.*[17]

In the present work we attempt to provide a consistent approach both in experiment and in subsequent modeling of neutron emission, utilizing a statistical model modified by the effects of nuclear dissipation. The compound nucleus we have chosen to investigate is ^{158}Er; we have previously performed extensive cross section measurements of a variety of projectile-target combinations leading to

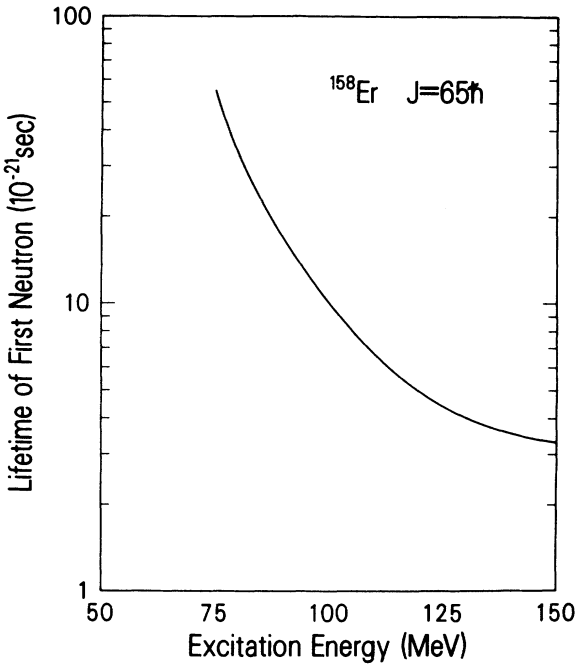

FIG. 1. Lifetime of the first neutron evaporated by ^{158}Er as a function of excitation energy.

this nucleus and have performed extensive statistical model calculations to interpret these data.[18,19] The wide variety of projectile-target combinations available enabled us to choose several combinations leading to very similar critical angular momenta but very different excitation energies. By varying the excitation energy we vary the average emission time of the first neutron $t_n^{(1)}=\hbar/\Gamma_n^{(1)}$ (Γ_n is the neutron decay width). The dependence of $t_n^{(1)}$ on the excitation energy is presented in Fig. 1 for an angular momentum of $65\hbar$ using standard statistical model calculations.[20] Thus a choice of excitation energy is equivalent to a choice of the speed of the neutron "clock." By changing $t_n^{(1)}$ and determining experimentally the average number of neutrons preceding fission, we will attempt to determine the time scale of the processes which increase the prefission neutron multiplicity. The list of reactions and bombarding energies we have chosen is presented in Table I. Our cross section measurements[18,19] (^{50}Ti+^{108}Pd reaction excepted) enable us to infer the limiting angular momentum for fission to be $(72-75)\hbar$. For the Ti + Pd reaction we use the Bass-1977 cross section value.[21] At these angular momenta the rotating finite range model (RFRM) fission barrier[22] is comparable to or greater than the temperature at the saddle point. This is a necessary condition for being able to apply the saddle point model for fission to these reactions[23] (assuming a compound nucleus is formed by the reaction inside the saddle point).

TABLE I. List of reactions and bombarding energies used in this work. E_b is the beam energy, E_x is the compound nucleus excitation energy. The asterisk denotes energy after emission of one nonequilibrium neutron (see text). $t_n^{(1)}$ is the lifetime of first neutron in cascade.

E_b (MeV)	Projectile	Target	E_x (MeV)	$t_n^{(1)}$ (10^{-21} s)
207	^{16}O	^{142}Nd	140*	3.5
180	^{24}Mg	^{134}Ba	115	5.4
180	^{32}S	^{126}Te	93	15
216	^{50}Ti	^{108}Pd	72	77

The prefission neutron multiplicities inferred from the data will be compared to modified statistical model calculations which incorporate the known effects of nuclear dissipation: (1) suppression of the fission probability[24] relative to the Bohr-Wheeler[25] value due to the Brownian nature of the motion to the saddle point, and (2) the finite time delay involved in the buildup of the fission probability at the saddle point. We use the model developed initially by Grangé and Weidenmüller[26] and expanded in Refs. 27 and 28. In addition, we calculate neutron emission during the transition from the saddlepoint to scission using the model of Hofmann and Nix.[29] By comparing our experimental values to the results of the model calculations, we obtain an estimate for the nuclear dissipation coefficient. Preliminary results of this work have been published in Ref. 2.

II. EXPERIMENT

The experiments were performed at the Holifield Heavy Ion Research Facility with coupled tandem-cyclotron operation. Typical beam intensities were approximately 1–2 nA. The targets used were oxides, $\sim$1 mg/cm^2 thick. In the first series of experiments (^{32}S, ^{50}Ti beams) fission fragments were detected in two position sensitive low-pressure multiwire proportional counter (MWPC) detectors[30] positioned at $\pm 60°$ to the beam axis for the ^{32}S beam and at $\pm 53°$ for the ^{50}Ti beam. The total in-plane angle subtended was 20°. The fission fragment detectors were mounted inside a 1.3 cm thick cylindrical aluminum scattering chamber having an inner radius of 77.5 cm. The neutron detectors, encapsulated NF213 scintillators, approximately 5 cm thick and 12 cm in diameter, were positioned immediately outside the chamber. Their angular positions are shown in Table II. In the second series of experiments (^{16}O, ^{24}Mg) a 40 cm radius, 0.3 cm thick spherical aluminum scattering chamber was used. The fission detectors were positioned at $+67°$ and $-65°$ to the beam axis and subtended an angle of 24° in plane. In addition, two evaporation-residue (ER) detectors were used in the second series of experiments, one on each side of the beam. Each ER detector was a 7×7 cm^2 double-gridded position sensitive low pressure MWPC, positioned 30 cm from the target. The ER detectors intercepted particles at in-plane angles between 3° and 17°. ER's were detected by measuring their time of flight (TOF) with respect to the cyclotron rf and considering their locus on a ΔE vs TOF plot. (ΔE is the anode signal in the ER detector.) Unfortunately, the ΔE resolution was insufficient to completely eliminate an underlying background of very slow beamlike particles which did not contribute to the neutron multiplicity but affected the overall normaliza-

TABLE II. Angles (in deg) of neutron detectors in first (I) and second (II) series of experiments. All detectors were in plane. Negative angle are on the left hand side with respect to the beam.

	Neutron detector no.									
	1	2	3	4	5	6	7	8	9	10
θ (in I)	146	105	60	31	14	−17	−32	−58	−75	−151
θ (in II)		131	75	61	26	−26	−47	−69	−99	−136

tion, especially in the ^{24}Mg run. The neutron detectors were placed approximately 70 cm from the target. Their angles are listed in Table II.

Neutron spectra in coincidence with fission fragments and evaporation residues were measured using TOF with respect to the cyclotron rf. The typical time resolution of the coupled tandem-cyclotron system was ~2 ns. The efficiency of the neutron detectors was determined by the procedure of Drosg[31] and normalized using the neutron spectrum in coincidence with fission fragments from a ^{252}Cf source in a 2π geometry. Typical normalization corrections were 20% in the first series (large scattering chamber) and $<10\%$ in the second series of experiments (3 mm thick scattering chamber). Pulse shape discrimination was used to reject gammas in the neutron TOF spectrum. The pulse shape signal was derived by subtracting the TOF obtained with zero crossing discriminators from the TOF obtained with constant fraction discriminators. Neutrons in coincidence with subsequent beam bursts were also recorded in order to obtain a correction for random coincidences. Pulse heights from the scintillators were recorded with the time of flight data to enable us to set a pulse height threshold consistent with our neutron energy threshold, which was 2 MeV. Below this energy, significant effects of neutron scattering could be discerned by considering the pulse-height trend as a function of energy. In addition, fluctuations in the photomultiplier gain rendered these data unreliable.

III. RESULTS—EVAPORATION RESIDUES

Figures 2 and 3 present neutron energy spectra in coincidence with evaporation residues from the 207 MeV ^{16}O+^{142}Nd reaction. As can be expected from reactions at these energies,[32,33] two components can be discovered in the spectra: (1) an evaporation component with a low (~2 MeV) temperature, essentially isotropic in the c.m. system, and (2) (at higher neutron energies) a high temperature, forward peaked nonequilibrium component. In this analysis, we assume that the shape of the spectrum of neutrons is given by

$$\phi(\epsilon)=\epsilon^{\alpha}e^{-\epsilon/T},$$

in the appropriate frame of reference: a frame moving with c.m. velocity $v_{\text{c.m.}}$ for the equilibrium neutrons and a frame with the moving source velocity v_{NE} for the nonequilibrium neutrons. Each source also has its own temperature: T_{eq} and T_{NE}, respectively. For the equilibrium

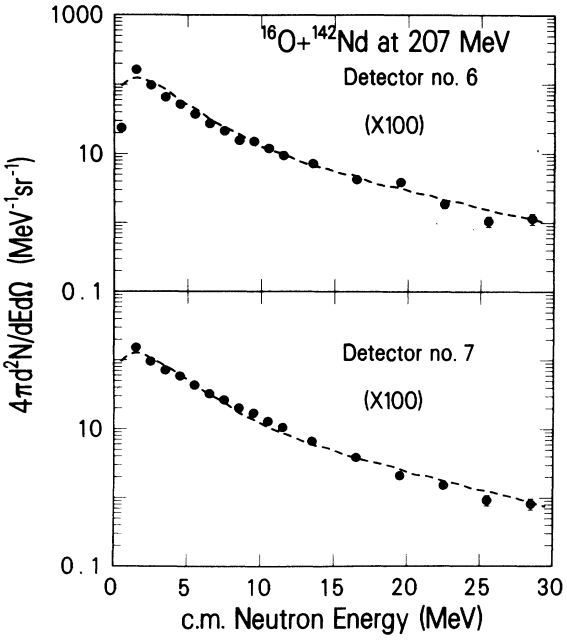

FIG. 2. Neutron spectra in the c.m. system, for the ^{16}O+^{142}Nd reaction in coincidence with evaporation residues. The dashed line is a result of a two source fit. Detector positions are presented in Table II.

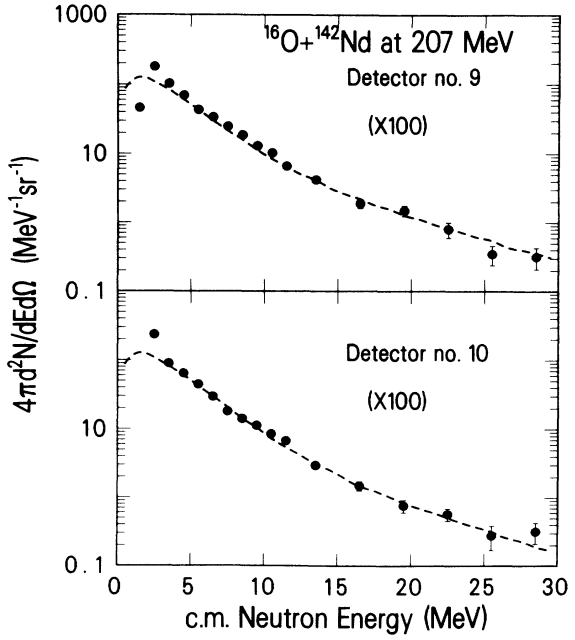

FIG. 3. Same as Fig. 1, for two additional detector positions.

source, the spectral shape obtained from evaporation calculations is $\epsilon^{0.6}e^{-\epsilon/T}$. For the NNE (nonequilibrium neutron) spectrum we have taken $\alpha=1$. In our subsequent analysis the term "temperatures" should be interpreted as the parameter T in our expression for $\phi(\epsilon)$ unless stated otherwise. Neutron emission and ER recoil are simulated using a Monte Carlo code. The simulation includes emission from the two neutron sources, the TOF resolution, the neutron detection efficiency, the ER recoil, and consequent selection due to the finite geometry of the ER detectors. Our simulation shows that the finite angular acceptance of the ER detectors in the experiment does not induce any significant bias in the neutron spectra or angular distribution. The neutron multiplicities we obtain by fitting the simulated spectra to the experimental data for the O + Nd reaction are $\bar{\nu}_{EQ}=5.7\pm0.2$ neutrons and $\bar{\nu}_{NE}=0.9\pm0.1$ neutrons. The associated temperatures are $T_{EQ}=1.9\pm0.2$ MeV and $T_{NE}=5.5\pm0.2$ MeV. We also find $v_{NE}=1.4\pm0.2$ cm/ns. The error in any given parameter was determined as the deviation from the value at the minimum of χ^2 which causes an increase of 10% in χ^2. We adopted this procedure in lieu of standard statistical formulae since the χ^2 values indicated significant systematic errors in our analysis. A single standard deviation in the neutron multiplicities, for instance, should only cause an increase of approximately 5% in χ^2.

T_{EQ} enables us to determine the "little-a" parameter in the Fermi gas level density model by fitting the exponential tail of the neutron evaporation spectrum obtained from the code PACE2.[20] We find $a=A/7.5$ for the ^{158}Er composite system. From these evaporation calculations (which include the effect of one nonequilibrium neutron preceding the evaporation cascade), we obtain $\bar{\nu}_{eq}=7.5$, significantly higher than our experimental result of 5.7 ± 0.2. There are two possible causes for this discrepancy: (1) Our normalization is erroneous due to contamination of our ΔE-TOF plot for residues by slow highly degraded beamlike particles. We have evidence for such an effect from the dependence of $\bar{\nu}_{EQ}$ on the (software) threshold used for the ΔE spectrum in the detectors. This effect was considerably worse for Mg induced reactions and, consequently, we do not present data using the Mg beam. (2) Incomplete fusion effects, specifically emission of fast alpha particles,[34] decrease the available energy for neutron emission. These effects are unimportant for the subsequent analysis. The fission fragment coincidence measurements are not contaminated by the low energy particles. In addition, incomplete fusion does not significantly precede fission in this reaction.[19] The parameters we subsequently use are a_n, which is used in the statistical model calculations, and v_{NE} and T_{NE}, which are used for the decomposition of nonequilibrium neutrons in coincidence with fission fragments.

IV. RESULTS—FISSION FRAGMENTS

In order to fit the neutron spectra in coincidence with fission fragments, three neutron sources were assumed: The first two sources were identical to those used in the analysis of ER's, namely nonequilibrium emission from a moving source and emission from the composite system. The third source was neutron emission from the fission fragments. The fragment source includes neutron emission during the acceleration of the fragments, using the procedure of Hinde *et al.*[7] We note, however, that for light composite systems (e.g., ^{158}Er) the effect of this procedure on the prefission multiplicity is less than 5%. Using Monte Carlo techniques identical to those used for the ER analysis, but including the mass and kinetic energy distributions of the fission fragments, we produce simulated spectra in the neutron detectors and determine the correct normalization of the three components by a least-squares fit to the data. Repeating this procedure for different prefission equilibrium temperatures T_{EQ} and different fission fragment temperatures T_{FF} (T_{NE} and v_{NE} are taken from the residue data), we are able to determine the values of $\bar{\nu}_{EQ}$, $\bar{\nu}_{NE}$, $\bar{\nu}_{FF}$, $\bar{\nu}_{EQ}$, and T_{FF} that minimize χ^2. The errors are deviations that cause an increase of 10% in the minimum χ^2.

Experimental neutron spectra in coincidence with the fission fragments are presented for all four reactions in Figs. 4—11. The lines depict simulated spectra using the parameters which give the best fit. These are presented in Table III. The fluctuations due to the finite statistics of the Monte Carlo calculations are clearly visible as structure in the lines.

In the first series of experiments, the spectra are com-

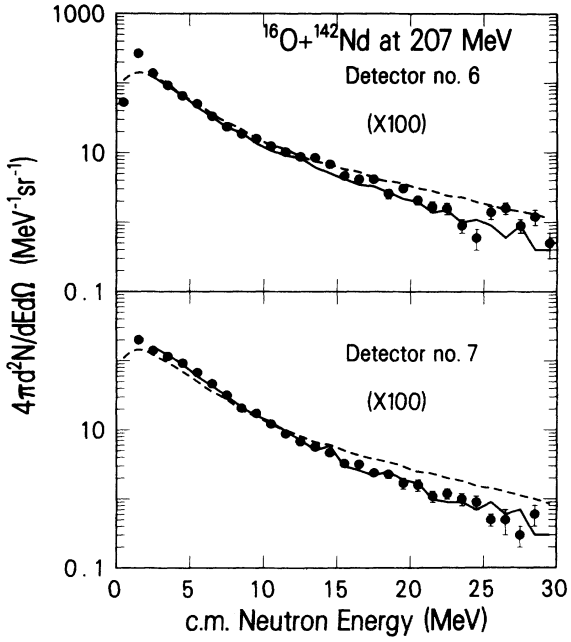

FIG. 4. Neutron spectra, in the c.m. system, for the ^{16}O + ^{142}Nd reaction, in coincidence with fission fragments. The solid line is a result of Monte Carlo simulation. The dashed line is a result of the two source fit to the spectrum in coincidence with evaporation residues. Note the enhancement of the experimental data at low energies in the direction of the fission fragments (detector no. 7), with respect to the dashed line. The enhancement is due to the neutrons evaporated from the fission fragments.

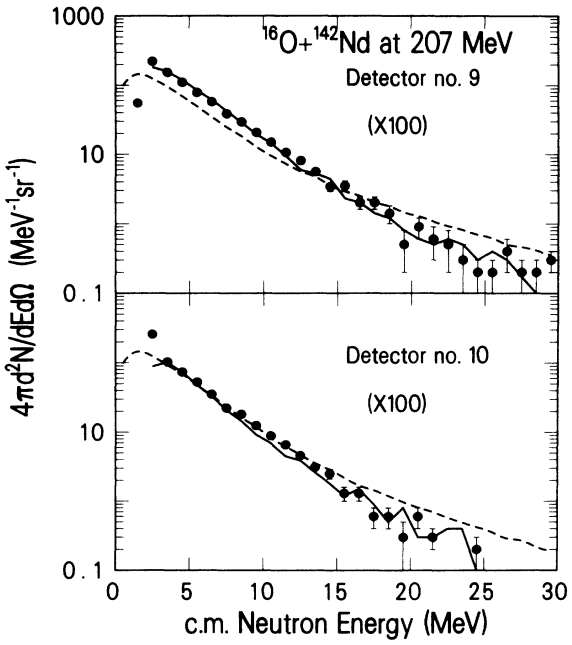

FIG. 5. Same as Fig. 3, for two additional detectors.

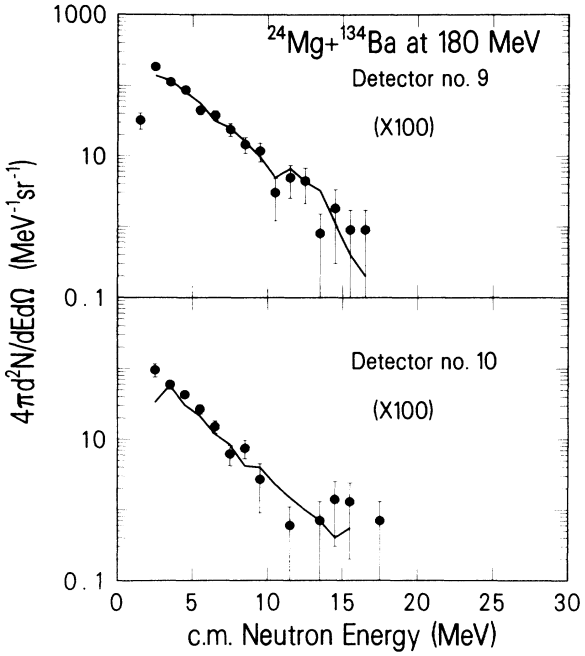

FIG. 7. Same as Fig. 5, for two additional detectors.

pared in the lab frame of reference (Figs. 8—11) and, in the second series, in the c.m frame (Figs. 4—7). The dashed line in Figs. 4 and 5 is the fit to the residue spectra using the moving source parametrization. The simulated spectra (solid line) deviate from the data both at low and at high energies: (1) At the very lowest energy threshold, fluctuations in the pulse height of signals from the neutron detectors cause significant discrepancies. (2) At the highest energies, the statistics of Monte Carlo simulation is poor. Neither of these problems has a significant effect on the main goal of this work—separation of the neutron spectra into prefission and postfission contributions.

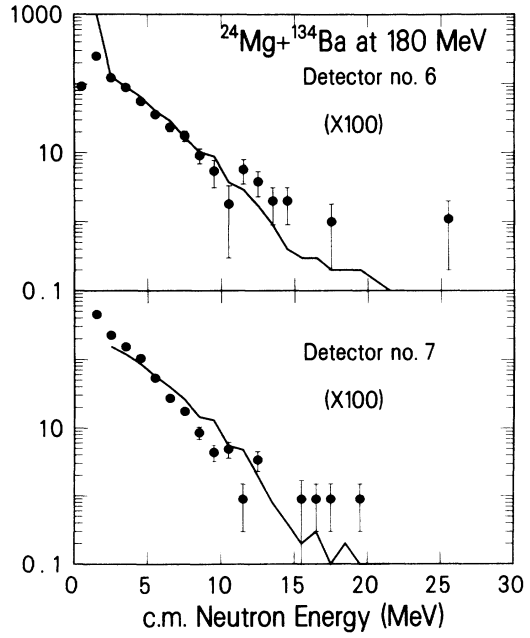

FIG. 6. Same as Fig. 3, for the ^{24}Mg + ^{136}Ba reaction.

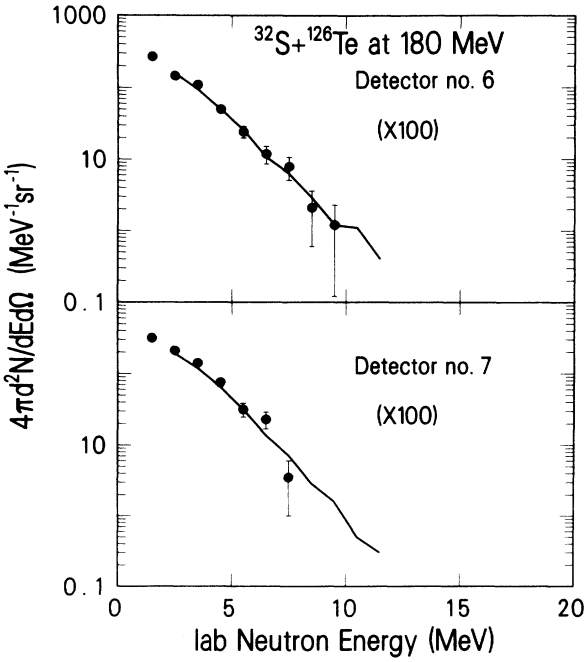

FIG. 8. Same as Fig. 3, ^{32}S + ^{126}Te reaction, in laboratory system.

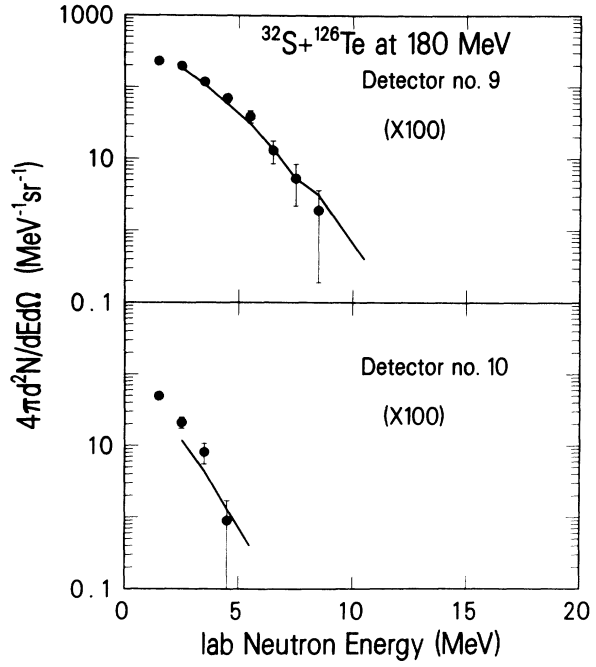

FIG. 9. Same as Fig. 7, for two additional detectors.

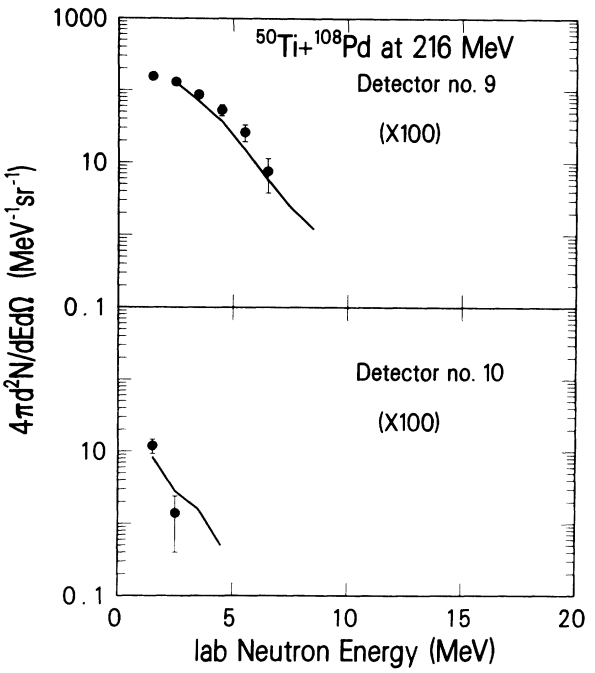

FIG. 11. Same as Fig. 9, two additional detectors.

V. DISCUSSION—EVAPORATION RESULTS

We compare the results of $\bar{\nu}_{NE}$, T_{NE}, and v_{NE} to systematics obtained for the ^{170}Yb system.[33] The energy per nucleon above the Coulomb barrier is 8.5 MeV/nucleon for $^{16}O+^{142}Nd$ at 207 MeV. Considering Fig. 1, Ref. 33, we expect a NNE multiplicity of 1–1.5 neutrons compared to our value of 0.9±0.1. Using the systematics of Fig. 3, Ref. 33, we predict $v_{NE}=1.5$ cm/ns, which agrees well with our result of 1.4±0.2 cm/ns. Equation (3) of Ref. 33 predicts $T_{NE}=4.7$ MeV, slightly lower than our experimental result of 5.5±0.2 MeV. We conclude that the systematics of Ref. 33 provide reasonable predictions of NNE emission with light projectiles, although minor discrepancies exist.

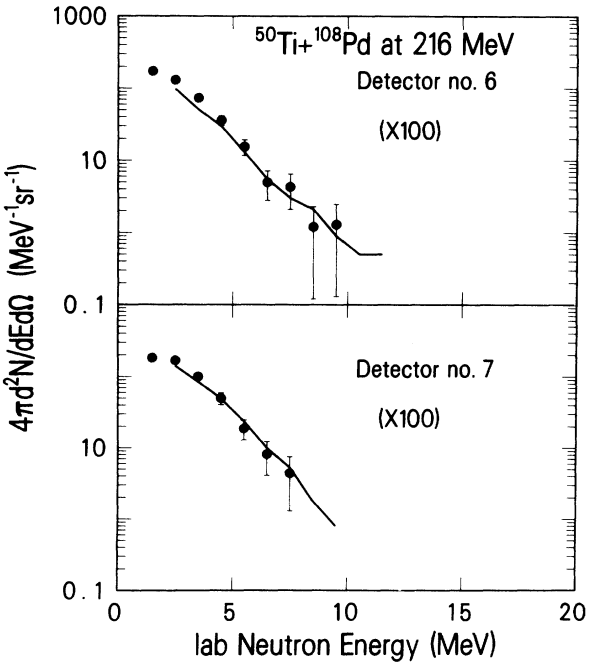

FIG. 10. Same as Fig. 7, $^{50}Ti+^{108}Pd$ reaction.

VI. DISCUSSION—FISSION FRAGMENTS

For the following analysis, we use our standard statistical model code[20] PACE2, which involves angular momentum dependent RFRM fission barriers.[22] Values of a_f/a_n were taken from Ref. 18, where the model was used to fit fission cross section data; $a_n=A/7.5$ was deduced from neutron spectra in coincidence with residues and with fission fragments. The critical angular momentum for fusion l_c was taken from Ref. 18. We constrained the calculated fission cross sections to be equal to the experimental values,[18,19] with the exception of the $^{50}Ti+^{108}Pd$ reaction, where the Bass-1977 value[21] was taken. The diffuseness in angular momentum of the partial wave distribution was also inferred from experimental data.[18]

Figure 12 presents comparisons of the experimental data to the statistical model calculated values for prefission neutron emission. In the upper half of the figure we see the well known discrepancy between calculated and measured prefission neutron multiplicities. On the other hand, there is no discrepancy at high energies, for the prefission neutron temperatures. The discrepancy for $^{32}S+^{126}Te$ could be due to effects of "quasi-fission,"[12–15] which cause part of the initial energy to be tied up in col-

TABLE III. Neutron multiplicities and temperatures of the different sources in coincidence with fission fragments. $\bar{\nu}$ is the average neutron multiplicity, T the temperature, NE the nonequilibrium neutron emission, EQ the compound nucleus evaporation, preceding fission, and FF the fission fragment emission. A number in parentheses implies that its value was not varied for the fit.

Reaction	$\bar{\nu}_{NE}$	T_{NE} (MeV)	$\bar{\nu}_{EQ}$	T_{EQ} (MeV)	$\bar{\nu}_{FF}$	T_{FF} (MeV)
^{16}O+^{142}Nd	0.9±0.1	(5.5)	2.7±0.4	2.3±0.1	1.9±0.2	1.4±0.1
^{24}Mg+^{134}Ba			2.5±0.5	2.0±0.1	1.8±0.2	1.1±0.1
^{32}S+^{126}Te			1.7±0.5	1.2±0.1	1.2±0.2	0.7±0.1
^{50}Ti+^{108}Pd			0.3±0.3	1.4±0.2	0.9±0.1	0.6±0.1

lective degrees of freedom for the duration of the reaction. In addition, one should also consider the possibility of bias to the data due to the large scattering chamber used for the ^{32}S and ^{50}Ti reactions. The ^{252}Cf calibration corrects for efficiency degradation in the chamber but not for multiple scattering effects. If the spectra in the backwardmost neutron detectors (nos. 1 and 10, see Table II) were affected significantly by scattering, this could account both for the high multiplicity and low temperature (the scattered neutron spectrum would be "soft"). However, no such effect is discernable in the ^{50}Ti+^{108}Pd reaction, which seems to rule out such a possibility.

Possible origins for the discrepancy in neutron multiplicities preceding fission have been pointed out by several groups.[1–8] We consider the discrepancy to be evidence for the existence of periods during the compound nucleus decay process when neutrons can be emitted but fission does not compete. Two such periods are evident.

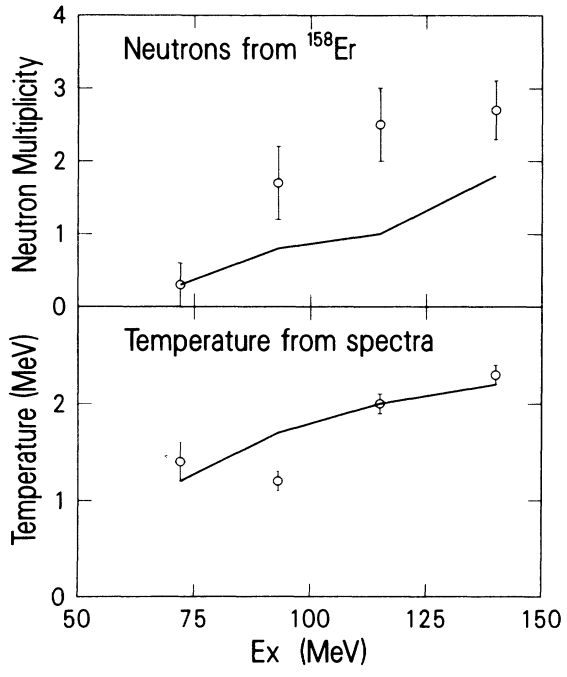

FIG. 12. Comparison between experimental results of the number of neutrons preceding fission and calculated values. The lower half of the figure shows a similar comparison for the temperature.

(1) At the time the compound nucleus is formed, the collective flow in the fission direction has not yet built up. Grangé *et al.*[27,28,35] have calculated the time it takes to build up the equilibrium value of Γ_f across the fission barrier ("transient time") as a function of the reduced nuclear dissipation coefficient β. This time has a minimum value of approximately 3×10^{-21} s for the ^{158}Er system with angular momentum of $65\hbar$, but could be an order of magnitude greater, depending on β. (See Fig. 14.) For $\beta\lesssim2\times10^{21}$ s^{-1} the system is underdamped. For larger values of β it is overdamped.

(2) During the descent from the saddle point down to scission, neutrons can be emitted from the hot nuclear matter. These neutrons will be considered "prefission" based on their temperature and angular distribution, but are not involved in the statistical competition between fission and neutron emission. The saddle-to-scission time varies typically between $(1-5)\times10^{-21}$ s, depending on dissipation and angular momentum.[35,36]

One can crudely estimate the total time involved in these processes by converting the difference between the measured and calculated neutron multiplicities to a time scale: We assign an average emission time $t_n^{(i)}=\hbar/\Gamma_n(i)$ to the ith neutron in the cascade. $\Gamma_n(i)$ is calculated at the remaining excitation energy left for the emission of the ith neutron. The time involved is then

$$\sum_{i=1}^{\bar{\nu}_{expt}} t_n^{(i)} - \sum_{i=1}^{\bar{\nu}_{calc}} t_n^{(i)} .$$

This estimate, for all four reactions, is presented in Fig. 13. Although the errors on the neutron multiplicity are approximately equal, their conversion to time entails much larger errors at lower excitation energies due to the much longer time associated with each neutron. The most accurate result is obtained from the ^{16}O+^{142}Nd reaction at 207 MeV: $(2-10)\times10^{-21}$ s. A more rigorous discussion of the time scales involved will be presented in the following sections.

VII. ANALYSIS

In order to be able to provide a comprehensive interpretation of the data, we introduce a modified statistical model which incorporates effects of nuclear dissipation. In addition, we calculate the multiplicity of neutrons emitted during the descent from the saddle to the scission point and add these to the pre-saddle-point neutrons

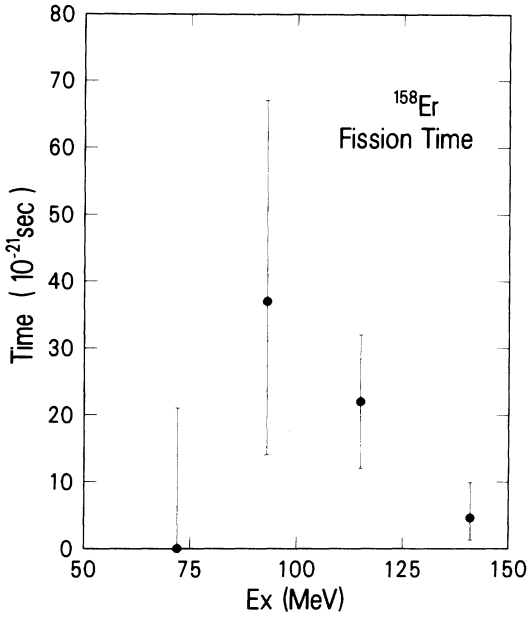

FIG. 13. Estimate of the "time scale of fission" for the four different reactions.

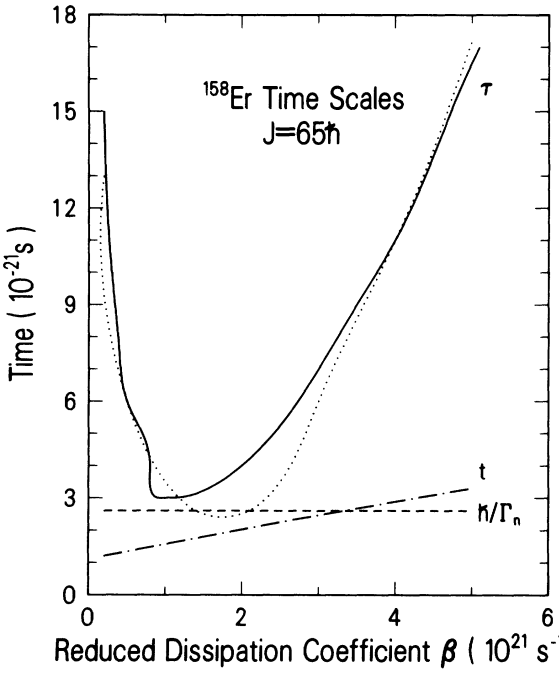

FIG. 14. Time scale of various processes. Curves marked τ are the transient time. The solid line is a result of the solution of the Fokker-Planck equation. The dotted line is the result of analytic approximation to the solutions. The dotted-dashed line (t) is the saddle-to-scission time. $\hbar/\Gamma_n$ is the average emission time of the first neutron.

which are in competition with fission.

The statistical model calculations are modified by the following two effects.

A. Transients

It has been pointed out by Grangé and Weidenmüller[26] (and later analyzed by them in detail[35]) that it takes a finite time to build up the quasi-stationary probability flow over the fission barrier. We define τ as the time necessary to reach 90% of the asymptotic value of Γ_f. For a particular compound nucleus and value of angular momentum, τ is a function of the nuclear dissipation: For very low values of the nuclear dissipation coefficient β, the coupling between the intrinsic and collective degrees of freedom is small, and consequently τ is large. For large values of β, the motion to the saddle point is overdamped and again τ is large. Figure 14 presents the transient time τ as a function of β calculated[35] by solving the Fokker-Planck equation[27,28] for the ^{158}Er compound nucleus with $J=65\hbar$ and $E_x=140$ MeV. The dotted line depicts transient times calculated using analytical approximations developed by Grangé and co-workers.[26–28,35] In our following calculations we have used these approximations to parametrize Γ_f as a function of time, for varying values of the compound nucleus mass, excitation energy, angular momentum, and the reduced dissipation coefficient. We note that, for most values of β, τ is large compared to the saddle-to-scission time t.

The transient effect is incorporated into our Monte Carlo statistical model calculations as follows: For each cascade, at each step in the decay chain (specific A, Z, E_x, J), an exponentially distributed particle decay time t_p is selected,

$$t_p=-\hbar/\Gamma_p \ln R \ ,$$

where R is a random number uniformly distributed between 0 and 1, and Γ_p is the total particle decay width. The cumulative time of this decay and all previous decays in this cascade, $t=\sum t_p$, is calculated, and used to compute $\Gamma_f(t)$. $\Gamma_f(t)$ is defined as the Kramers value of Γ_f multiplied by the ratio of the flux at time t over the barrier to the flux at infinite time.[35] The probability of fission at this step is just $\Gamma_f(t)/[\Gamma_p+\Gamma_f(t)]$.

This ansatz contains an important implicit assumption—that there is indeed a time zero at which the internal degrees of freedom have been completely equilibrated. At this time (and not before) particle emission can start (with its full width Γ_p), and the Brownian motion of the nucleus towards the saddle point also commences. In practice, we are ignoring the (plausible) possibility that Γ_p attains a finite value *during* the equilibration process of the compound nucleus. Clear evidence for such an effect is the observation of nonequilibrium emission in the ^{16}O+^{142}Nd reaction. We circumvent this effect by assuming that the detected neutrons can be decomposed into three *distinct* components: nonequilibrium, equilibrium prefission, and equilibrium postfission. These processes, in reality, evolve continuously and a more complete analysis can be achieved only by a full calculation from the time the incident ions interact until they have completed deexcitation.

B. Steady stage value of Γ_f

Γ_f has usually been determined using the Bohr-Wheeler[25] formalism. One of the basic assumptions in this formalism is that nuclei decaying from the ground state toward fission all pass over the saddle point and continue down to scission. However, due to the Brownian nature of the motion, some nuclei are reflected back to the ground state; this can happen even after they have passed over the saddle point. This has been considered by Kramers,[24] who obtained a modified value of Γ_f from a steady state solution to the Fokker-Planck equation:

$$\Gamma_f = \Gamma_f^{\mathrm{BW}}\{[1+(\beta/2\omega)^2]^{1/2}-\beta/2\omega\} .$$

Γ_f^{BW} is the value of Γ_f determined by the Bohr-Wheeler formalism, β the reduced dissipation coefficient, and ω the curvature of the fission barrier at the saddle point. For $\beta>0$, Γ_f decreases monotonically with β, and is less than Γ_f^{BW}.

The two modifications—transient effects and Kramers correction—assign a lower effective value to Γ_f compared to our previous statistical model calculations. The immediate implication is that we have to redetermine a_f/a_n to fit the experimental values of σ_{fiss} prior to any further calculation of neutron emission. The values of a_f/a_n that reproduce σ_{fiss} are represented in Fig. 15 as a function of β. The solid line depicts a_f/a_n disregarding transient effects (Kramers correction only). The dashed line shows the final value including both the effects. These are the values used in subsequent calculations.

The multiplicity of neutrons emitted during the saddle-to-scission transition is calculated as follows: For each event that goes to fission in the statistical model calculation (specific A, Z, E_x, and J), we calculate Γ_n based on an effective excitation energy at the saddle point. The effective excitation energy E_{eff} is defined as follows:

$$E_{\mathrm{eff}} = E_x - E^s_{\mathrm{rot}}(J) + \Delta E .$$

$E^s_{\mathrm{rot}}(J)$ is the rotational energy at the saddle point and ΔE is half the increase in excitation energy during the saddle-to-scission transition as determined by the model of Hoffman and Nix.[29] The average saddle-to-scission time $\bar{\tau}$ is determined using the same model. Given $\bar{\tau}$ and $t_n = \hbar/\Gamma_n$, we calculate the multiplicity of neutron emission during the descent to scission for this event. On an event-by-event basis, there is an almost complete anticorrelation between neutron multiplicity due to the transient effect and the number of neutrons emitted after the saddle point. For high partial waves, the fission barrier is very low and first chance fission is dominant. The descent from the saddle point takes place at a high temperature, which gives rise to 1—2 neutrons emitted during this transition. For low partial waves, second or third chance fission is dominant, and the low temperature at the saddle point precludes significant neutron emission during the descent.

We present a comparison of calculated values of neutron emission, as a function of β in Figs. 16—19, compared to experimental results. The limits of the experimental results are represented by the two horizontal dashed lines. Statistical model calculations using the Bohr-Wheeler formalism are depicted by the dotted line (marked SM). Including the effect of transients and Kra-

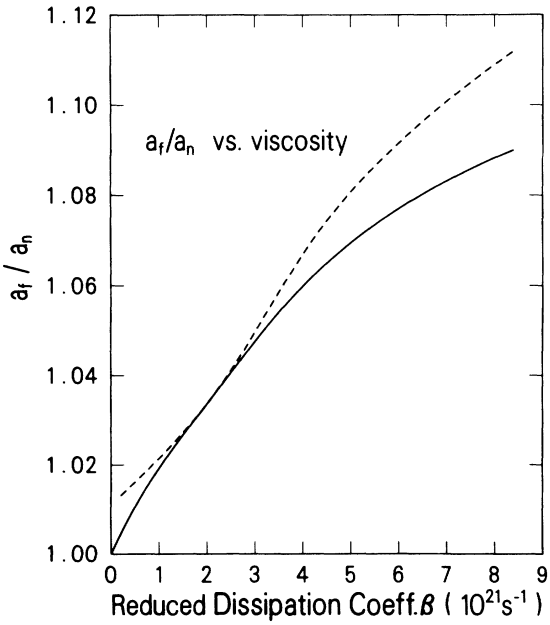

FIG. 15. Values of a_f/a_n that reproduce the fission cross section as functions of β. The solid line is obtained using the Kramers correction. The dashed line includes transient effects.

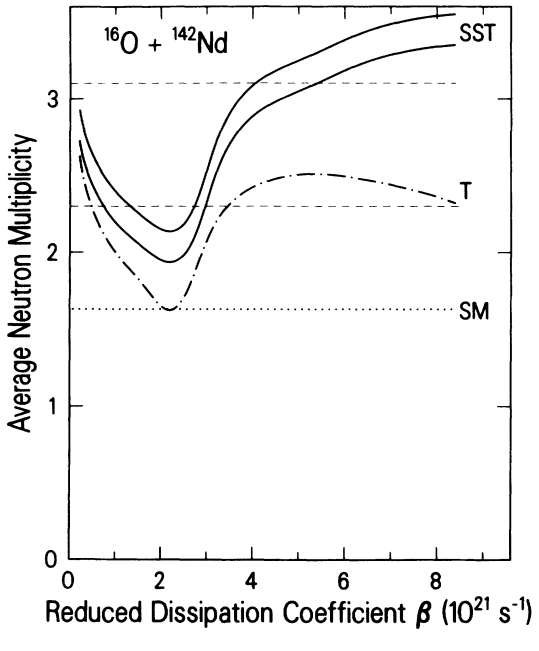

FIG. 16. Comparison of experimental results to model calculations for the $^{16}O+^{142}Nd$ reaction. The two horizontal dashed lines depict upper and lower limits of the experimental data. The two solid lines describe the upper and lower limits of the model calculations (SST). The curve marked T (dashed-dotted) excludes saddle-to-scission neutrons. The dotted curve (SM) is the result of statistical model calculations using the Bohr-Wheeler formalism.

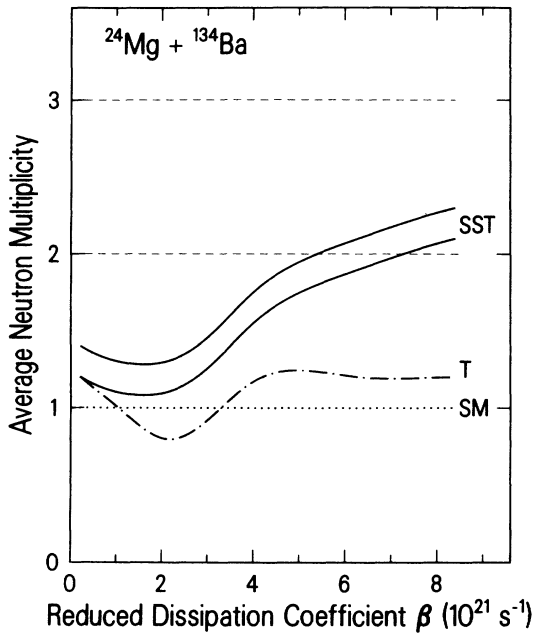

FIG. 17. Same as Fig. 15, for the ^{24}Mg+^{134}Ba reaction.

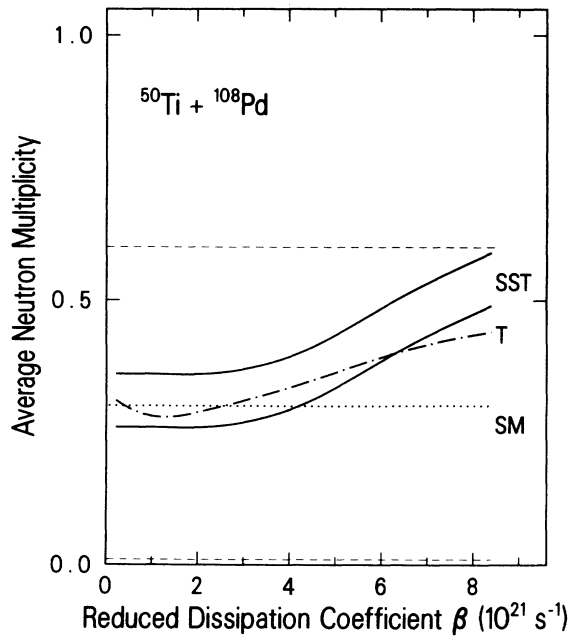

FIG. 19. Same as Fig. 15, for the ^{50}Ti+^{108}Pd reaction.

mers correction (and using a_f/a_n as a function of β), we obtain the dashed-dotted curve marked T. Adding neutrons emitted during the saddle-to-scission transition, we obtain the solid curves marked SST. The two curves are the upper and lower limits of the calculated values. These limits are the result of (1) the uncertainty in the fission cross section used as input to determine the critical angular momentum, (2) the use (or omission) of shell and pairing corrections to the mass and level densities, and (3) errors in the value of a_n used.

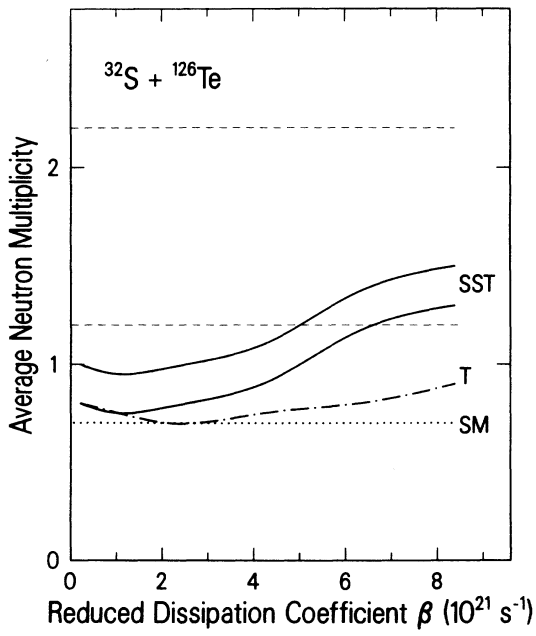

FIG. 18. Same as Fig. 15, for the ^{32}S+^{126}Te reaction.

For ^{16}O+^{142}Nd (Fig. 16), there are two ranges of β values for which there is agreement between experimental results and our model calculation: $3\lesssim\beta\lesssim 6$ and $\beta\lesssim 1.5$ (in units of 10^{21} s^{-1}). However, given the size of the experimental errors and the uncertainty of the model calculations, we do not consider the intermediate region of $\beta\sim 2\times 10^{21}$ s^{-1} to be excluded by the data. From the ^{16}O+^{142}Nd reaction we deduce that $\beta\lesssim 6\times 10^{21}$ s^{-1}. The ^{24}Mg+^{134}Ba and ^{32}S+^{126}Te reactions (Figs. 16 and 17) enable us to deduce a lower limit of $\beta\gtrsim 5\times 10^{21}$ s^{-1}. The ^{50}Ti+^{108}Pd reaction (Fig. 18) shows agreement for all values of β in this range. The results we have obtained thus imply $\beta\sim 6\times 10^{21}$ s^{-1} for the ^{158}Er composite system, assuming that β is independent of temperature,[29,37] within the framework of this model.

We now attempt to estimate the time delay, actually involved in the transient effect: For low partial waves ($l\lesssim 65\hbar$) the particle decay width $\Gamma_n(l)$ is larger than the asymptotic value of the fission decay width $\Gamma_f(l)$; consequently, fission will most probably occur when Γ_f approaches its asymptotic value. For $\beta=6\times 10^{21}$ s^{-1} this is after $\sim 30\times 10^{-21}$ s. For larger values of l, the fission barrier is lower, and therefore $\Gamma_f(l,t)$ can exceed $\Gamma_p(l)$ at times that can be short relative to the transient time τ. This is depicted in Fig. 20, where $\Gamma_f(l,t)/\Gamma_f(l,t=\infty)$ is plotted as a function of t for $l=65\hbar$, $70\hbar$, and $75\hbar$. The horizontal straight lines depict $\Gamma_p(l)/\Gamma_f(l,t=\infty)$ on this scale for the three partial waves. For $l=70\hbar$, Γ_f exceeds Γ_p when t is greater than 18×10^{-21} s; for $l=75\hbar$ the crossing point occurs at $t=5\times 10^{-21}$ s, which is much less than τ. Thus even though we are considering a system with finite barriers for all partial waves, the composite system can fission before the fission degree of freedom is equilibrated. As l increases above $65\hbar$, this possibility becomes more and more significant. The fission degree of

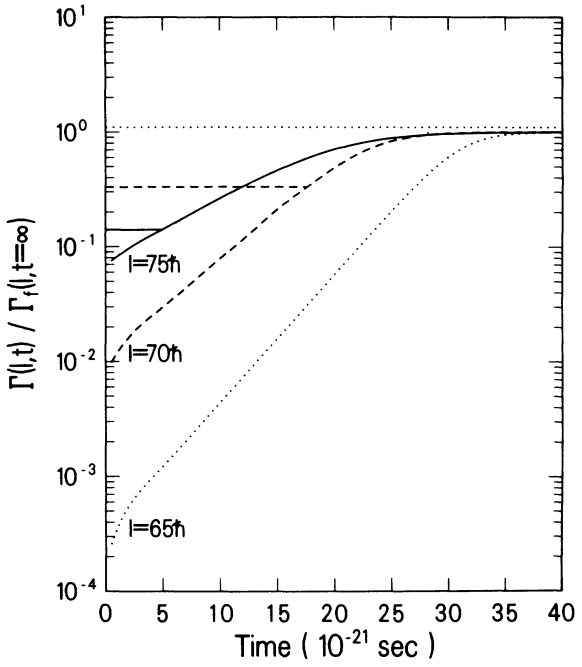

FIG. 20. Calculated decay widths as a function of time. Horizontal lines are $\Gamma_p(l)$. Curved lines are $\Gamma_f(l,t)$. The dotted line is for 65$\hbar$, the dashed line for 70$\hbar$, and the solid line for 75$\hbar$.

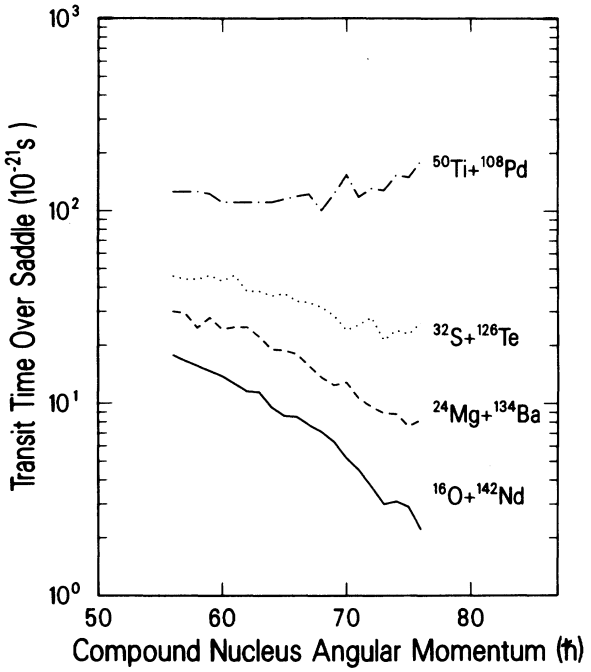

FIG. 21. The average transit time duration until the nucleus passes over the saddle point, as a function of angular momentum. The results were obtained our modified statistical model calculations. The fluctuations are due to the finite statistics of our Monte Carlo calculations.

freedom decays prior to attaining equilibrium even though we assumed that the system was formed inside the saddle point and was completely equilibrated in all the internal degrees of freedom. This effect should be considered in connection with nonequilibrium angular distribution results observed in certain fission reactions.[13–15] It is not clear why one reaction provides an upper limit to β, whereas other reactions provide a lower limit. It is possible that this effect too could be due to dynamic effects which are sensitive to specific reaction partners for heavy projectiles or, of course, to shortcomings in the model we use to calculate $\Gamma_f(t)$. The actual transit time (defined as the average time duration until the compound nucleus passes over the saddle point) is presented in Fig. 21 for the four reactions as a function of angular momentum. The results were obtained using our modified statistical model in which time is followed for each cascade. The fluctuations in the curves are due to the finite statistics of the Monte Carlo simulation. For the $^{16}O+^{142}Nd$ reaction, the transit time is 8×10^{-21} s for 65$\hbar$, dropping down to 3×10^{-21} s for 75$\hbar$. If we add the saddle-to-scission time,[25] the total time scale is 12×10^{-21} s for 65$\hbar$ and 9×10^{-21} s for 75$\hbar$, assuming $\beta=6\times10^{21}$ s^{-1}. From the other reactions, we conclude that the lower the excitation energy, the longer the time scale. A more rigorous approach to determining the time scale of fission thus confirms the general results of Fig. 13, with the exception of the $^{50}Ti+^{108}Pd$ reaction.

Summarizing, we have measured neutron emission preceding fission in the ^{158}Er composite system at various temperatures. The enhanced neutron emission relative to statistical model calculations can be attributed to dynamic effects of dissipation on the fission width and to neutron emission during the saddle-to-scission transition. If we assume that dissipation is temperature independent and that the time scale of fission is not influenced by the incoming projectile, one can deduce that $\beta\sim6\times10^{21}$ s^{-1}, within the framework of the specific model we have used.[35] This implies that the motion of a nucleus along the fission coordinate is overdamped. Further experiments on other systems will be necessary to corroborate this value. For this value of β, the average transit time over the saddle point is $\sim10^{-20}$ s for 207 MeV $^{16}O+^{142}Nd$. The saddle-to-scission time is $\sim5\times10^{-21}$ s.

[1]A. Gavron, J. R. Beene, B. Cheynis, R. L. Ferguson, F. E. Obenshain, F. Plasil, G. R. Young, G. A. Pettit, R. Jääskeläinen, D. G. Sarantites, and C. F. Maguire, Phys. Rev. Lett. **47**, 1255 (1981); **48**, 835(E) (1982).

[2]A. Gavron, A. Gayer, J. Boissevain, H. C. Britt, J. R. Nix, A. J. Sierk, P. Grangé, S. Hassani, H. A. Weidenmüller, J. R. Beene, F. Plasil, G. R. Young, G. A. Petitt, and C. Butler, Phys. Lett. **176B**, 312 (1986).

[3]D. Hilscher, E. Holub, U. Jahnke, H. Orf, and H. Rossner, in *Proceedings of the Third Adriatic Europhysics Study Conference,* Hvar, Yugoslavia, 1981, edited by N. Cindro, R. A. Ricci, and W. Greiner (North-Holland, Amsterdam, 1981), p. 225.

[4]E. Holub, D. Hilscher, G. Ingold, U. Jahnke, H. Orf, and H. Rossner, Phys. Rev. C **28**, 252 (1983).

[5]W. P. Zank, D. Hilscher, G. Ingold, U. Jahnke, M. Lehmann, and H. Rosner, Phys. Rev. C **33**, 519 (1986).

[6]D. Ward, R. J. Charity, D. J. Hinde, J. R. Leigh, and J. O. Newton, Nucl. Phys. **A403**, 189 (1983).

[7]D. J. Hinde, R. L. Charity, G. S. Foote, J. R. Leigh, J. O. Newton, S. Ogaza, and A. Chatterjee, Phys. Rev. Lett. **52**, 986 (1984); **53**, 2275(E) (1984).

[8]D. J. Hinde, R. L. Charity, G. S. Foote, J. R. Leigh, J. O. Newton, S. Ogaza, and A. Chatterjee, Nucl. Phys. **A452**, 550 (1986).

[9]E. Duek, N. N. Ajitanand, John M. Alexander, D. Logan, M. Kildir, L. Kowalski, Louis C. Vaz, D. Guerreau, M. S. Zisman, Morton Kaplan, and D. J. Moses, Z. Phys. A **317**, 83 (1984).

[10]Louis C. Vaz, D. Logan, E. Duek, John M. Alexander, M. F. Rivet, M. S. Zisman, Morton Kaplan, and J. W. Ball, Z. Phys. A **315**, 169 (1984).

[11]L. Schad, H. Ho, G. Y. Fan, B. Lindl, A. Pvoh, R. Wolski, and J. R. Wurm, Z. Phys. A **318**, 179 (1984).

[12]C. Lebrun, F. Hanappe, J. F. Lecolley, F. Levebres, C. Ngo, J. Peter, and B. Tamain, Nucl. Phys. **A321**, 207 (1979).

[13]J. Toke, R. Bock, G. X. Dai, A. Gobbi, S. Gralla, K. D. Hildenbrand, J. Kuzminski, W. F. J. Müller, A. Olmi, and H. Stelzer, Nucl. Phys. **A440**, 327 (1985).

[14]B. B. Back, Phys. Rev. C **31**, 2104 (1985).

[15]K. Lützenkirchen, J. V. Kratz, G. Wirth, W. Brüchle, K. Sümmerer, R. Lucas, J. Poitou, and C. Grégoire, Nucl. Phys. **A452**, 351 (1986).

[16]J. Blocki, Y. Boneh, J. R. Nix, J. Randrup, M. Robel, A. J. Sierk, and W. J. Swiatecki, Ann. Phys. (N.Y.) **113**, 330 (1978).

[17]K. T. R. Davies, A. J. Sierk, and J. R. Nix, Phys. Rev. C **13**, 2385 (1976).

[18]J. vanderPlicht, H. C. Britt, M. M. Fowler, Z. Fraenkel, A. Gavron, J. B. Wilhelmy, F. Plasil, T. C. Awes, and G. R. Young, Phys. Rev. C **28**, 2022 (1983).

[19]A. Gavron, J. Boissevain, H. C. Britt, K. Eskola, P. Eskola, M. M. Fowler, H. Ohm, J. B. Wilhemly, T. C. Awes, R. L. Ferguson, F. E. Obsenshain, F. Plasil, G. R. Young, and S. Wald, Phys. Rev. C **30**, 1550 (1984).

[20]A. Gavron, Phys. Rev. C **21**, 230 (1980).

[21]R. Bass, Phys. Rev. Lett. **38**, 265 (1977).

[22]A. J. Sierk, Phys. Rev. C **33**, 2039 (1986).

[23]V. M. Strutinskii, Yad. Fiz. **19**, 195 (1974) [Sov. J. Nucl. Phys. **19**, 127 (1974)].

[24]H. A. Kramers, Physica **7**, 284 (1940).

[25]N. Bohr and J. A. Wheeler, Phys. Rev. **56**, 426 (1939).

[26]P. Grangé and H. A. Weidenmüller, Phys. Lett. **96B**, 26 (1980).

[27]P. Grangé, Li Jun-Qing, and H. A. Weidenmüller, Phys. Rev. C **29**, 2063 (1983).

[28]K. H. Bhatt, P. Grangé, and B. Hiller, Phys. Rev. C **33**, 954 (1986).

[29]H. Hofmann and J. R. Nix, Phys. Lett. **122B**, 117 (1983).

[30]J. vanderPlicht and A. Gavron, Nucl. Instrum. Methods **24**, 403 (1983).

[31]M. Drosg, Nucl. Instrum. Methods **105**, 582 (1972).

[32]A. Gavron, J. R. Beene, R. L. Ferguson, F. E. Obenshain, F. Plasil, G. R. Young, G. A. Petitt, K. A. Geoffroy-Young, M. Jääskeläinen, D. G. Sarantites, and C. F. Maguire, Phys. Rev. C **24**, 2048 (1981).

[33]A. Gavron, J. R. Beene, B. Cheynis, R. L. Ferguson, F. E. Obenshain, F. Plasil, G. R. Young, G. A. Petitt, C. F. Maguire, D. G. Sarantites, M. Jääskeläinen, and G. Geoffroy-Young, Phys. Rev. C **27**, 450 (1983).

[34]K. Siwek-Wilczynska, E. H. du Marchie van Voorthuysen, J. van Popta, R. H. Siemssen, and J. Wilczynski, Nucl. Phys. **A330**, 150 (1979); J. Wilczynsksi, K. Siwek-Wilczynska, J. van Diel, S. Gonggrizp, D. C. J. M. Hageman, R. V. F. Janssens, J. Tukasiak, and R. H. Siemssen, Phys. Rev. Lett. **45**, 606 (1980).

[35]P. Grangé, S. Hassani, H. A. Weidenmüller, A. Gavron, J. R. Nix, and A. J. Sierk, Phys. Rev. C **34**, 209 (1986).

[36]J. R. Nix, A. J. Sierk, H. Hofmann, F. Scheuter, and D. Vautherin, Nucl. Phys. **A424**, 239 (1984).

[37]J. R. Nix, private communication.